https://doi.org/10.1016/j.engstruct.2023.117193

Ultra-High-Strength Engineered Cementitious Composites (UHS-ECC) Panel Reinforced with FRP Bar/Grid: Development and Flexural Performance

Ji-Xiang Zhu [1]; Ke-Fan Weng [2]; Bo-Tao Huang [3] (*); Ling-Yu Xu [4]; Jian-Guo Dai [5] (*)

Highlights

- FRP-reinforced UHS-ECC panel was developed and investigated for the first time.
- The load capacity of the UHS-ECC panel was 139–173% higher than that of the UHSC panel with the same reinforcement.
- Using UHS-ECC to replace UHSC significantly improved the effective strain of FRP.
- Owing to the tensile strain-hardening and multiple cracking behavior, UHS-ECC improved the stress transfer and deformation compatibility with FRP.
- The load capacities of the developed panels were predicted by an analytical approach.

[1] Ph.D. Candidate, Department of Civil and Environmental Engineering, The Hong Kong Polytechnic University, Kowloon, Hong Kong, China. E-mail: ji-xiang.zhu@connect.polyu.hk

[2] Ph.D. Candidate, Department of Civil and Environmental Engineering, The Hong Kong Polytechnic University, Kowloon, Hong Kong, China; Department of Ocean Science and Engineering, Southern University of Science and Technology, Shenzhen, Guangdong, China. E-mail: ke-fan.weng@connect.polyu.hk

[3] Research Fellow, Department of Civil and Environmental Engineering, The Hong Kong Polytechnic University, Hong Kong, China; ZJU100 Young Professor, Institute of Advanced Engineering Structures, Zhejiang University, Hangzhou, China. E-mail: botaohuang@zju.edu.cn (**Corresponding Author*)

[4] Postdoctoral Fellow, Institute of Advanced Engineering Structures, Zhejiang University, Hangzhou, China. E-mail: lingyuxu@zju.edu.cn

[5] Professor, Department of Civil and Environmental Engineering, The Hong Kong Polytechnic University, Hong Kong, China. E-mail: cejgdai@polyu.edu.hk (**Corresponding Author*)

ABSTRACT

In this study, Ultra-High-Strength Engineered Cementitious Composites (UHS-ECC) panels with Fiber-Reinforced Polymer (FRP) reinforcement (i.e., FRP bars and girds) were proposed for the construction of sustainable marine structures. Based on four-pointed bending tests, the mechanical performance of FRP-reinforced UHS-ECC [with 2% polyethylene (PE) fibers] and FRP-reinforced ultra-high-strength concrete (UHSC, without fibers) panels were investigated and compared to understand the composite action between UHS-ECC and FRP. Compared with the FRP-reinforced UHSC panel, the FRP-reinforced UHS-ECC panel showed significantly higher ultimate load (139%–173% higher), stiffness, and deformation capacity. It was also found that the use of seawater as the raw material had almost no effect on the mechanical performance of FRP-reinforced UHS-ECC (UHSC) panels. An analytical investigation was conducted to predict the load capacities of the tested panels, and the prediction error was acceptable. For FRP-reinforced UHS-ECC (UHSC) panels, it was revealed that using UHS-ECC to replace UHSC improved the stress transfer and deformation compatibility with FRP because the multiple cracking behavior of UHS-ECC lowered the crack-induced shear stress concentration along the FRP reinforcement. The developed FRP-reinforced UHS-ECC system showed great potential in the construction of durable and sustainable marine infrastructure.

KEYWORDS

Ultra-High-Strength Engineered Cementitious Composites (UHS-ECC); Strain-Hardening Cementitious Composites (SHCC); Ultra-High-Performance Concrete (UHPC); Ultra-High-Strength Concrete (UHSC); Fiber-Reinforced Polymer (FRP); Seawater; Composite Action; Multiple Cracking

1 Introduction

Reinforced concrete (RC) structures have been widely used in construction work [1] [2] [3] [4]. By combining concrete and steel reinforcement, the RC system has high cost-efficiency and good mechanical performance to meet the economical and safety requirements of most engineering structures. However, for marine and coastal construction [5] [6], the low corrosion resistance of steel reinforcement and the quasi-brittle behavior of concrete are the major limitations of RC structures [7] [8] [9]. In addition, marine structures have to sustain complex/extreme loadings (e.g., cyclic, fatigue, and impact loadings [10] [11] [12] [13] [14]). Therefore, it is meaningful to look for alternative advanced materials for the substitution of steel reinforcement and conventional concrete to develop safer, more durable, and more sustainable marine infrastructure.

Fiber Reinforced Polymers (FRP) reinforcement has become a suitable alternative to conventional steel reinforcement as this material possesses a high strength-to-weight ratio and excellent corrosion resistance [15] [16] [17] [18] [19] [20]. However, compared to RC members with the same cross-section and reinforcement details, FRP-reinforced concrete members still face several problems such as large crack width [21] [22] [23] and abrupt brittle failure [24] [25] [26], owing to the comparatively low elastic modulus and linear elastic characteristics of FRP materials. To address challenges, the conventional concrete layer can be replaced by Engineered Cementitious Composites (ECC) [27] [28] [29] [30] [31] [also termed as Strain-hardening Cementitious Composites (SHCC) [32] [33] [34] [35] [36] or Ultra-High-Toughness Cementitious Composites (UHTCC) [37] [38]] to enhance the crack resistance and ductility of the FRP-reinforced member [39] [40] [41].

ECC materials with tensile strain-hardening characteristics and multiple cracking ability are designed under the guidance of the micromechanical design principle [42] [43] [44] [45] [46].

Through the utilization of high-performance synthetic fibers [e.g., polyvinyl alcohol (PVA) fiber and polyethylene (PE) fiber], ECC can possess a high/ultra-high tensile ductility (typically 3–10%) several hundred times that of conventional concrete [47] [48] [49] [50]. In recent years, by combining the Ultra-High-Performance Concrete (UHPC) technology and the micromechanics-based design method of ECC, high-strength ECC (HS-ECC, 80–150 MPa) and ultra-high-strength ECC (UHS-ECC, 150–210 MPa) have been successfully designed and developed (see **Fig. 1**) [51] [52] [53]. These innovative materials successfully overcame the quasi-brittleness of conventional concrete and possessed higher mechanical performance and better durability due to the densified microstructures [54] [55] [56] [57]. It should be pointed out that one important advantage of the FRP-reinforced HS/UHS-ECC is that the high/ultra-high compressive strength is beneficial to improve the material efficiency of FRP reinforcement.

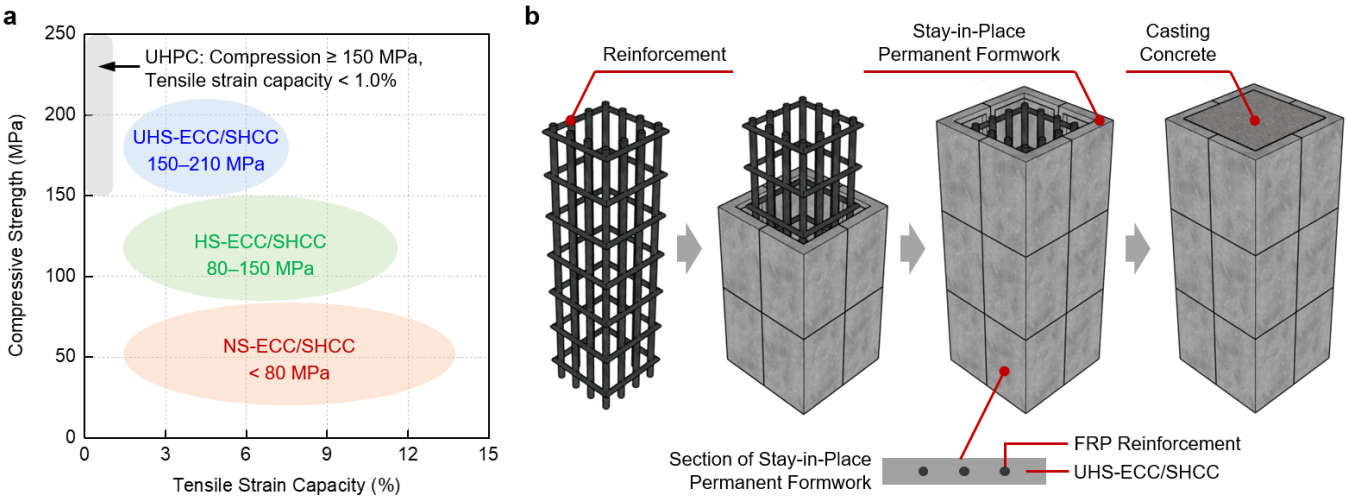

Fig. 1 (a) Mechanical properties of existing ECC materials; and (b) Schematic diagram of the stay-in-place permanent formwork made by FRP-reinforced UHS-ECC for marine and coastal applications.

It should be pointed out that FRP-reinforced UHS-ECC members are much more expensive than conventional RC members. Thus, using FRP-reinforced UHS-ECC as the exterior protective layer

could be a cost-effective solution for practical applications. As shown in **Fig. 1b**, FRP-reinforced UHS-ECC can be used to prefabricate stay-in-place permanent formwork for concrete members. In this system, the FRP-ECC layer serves as the stay-in-place permanent formwork during concrete casting, and they are also the exterior protective layer of the concrete member for its remaining life [58]. This strategic utilization of FRP-reinforced UHS-ECC could minimize the material cost and improve construction efficiency. It is worth mentioning that in marine and coastal regions, the FRP-ECC formwork system could also be used in the construction of seawater sea-sand concrete structures. In such a case, the UHS-ECC can be mixed with seawater directly, as the internal FRP reinforcements are non-corrosive [59]. Thus, the FRP-reinforced UHS-ECC panel shows great potential in the construction of durable and sustainable marine infrastructure.

It should be pointed out that the stay-in-place permanent formwork made by FRP-reinforced UHS-ECC in **Fig. 1b** is a schematic diagram of such potential application. This study focused on the flexural performance of FRP-reinforced UHS-ECC panels to demonstrate the feasibility of this newly proposed system. In addition, the understanding of the mechanical behavior and composite action of FRP-reinforced UHS-ECC panels is critical for the practical application. In the following parts, the flexural performance of the FRP-reinforced UHS-ECC panel was experimentally and theoretically investigated to understand the interaction between these two advanced engineering materials. Two types of FRP reinforcements (i.e., FRP bar and FRP gird) were used to reinforce the UHS-ECC panels, and their mechanical properties were tested using four-point bending tests with the assistance of Digital Image Correlation (DIC) techniques. The test results were compared to those of FRP-reinforced Ultra-High-Strength Concrete (UHSC) panels (without fibers). In addition, the influence of seawater on the mechanical performance of FRP-reinforced UHS-ECC panel systems was also evaluated. Finally, an analytical investigation was conducted to predict the load capacities of the FRP-

reinforced UHS-ECC (UHSC) panels.

2 Experimental programs

2.1 Ultra-High-Strength ECC (UHS-ECC)

The mix proportions of UHS-ECC and Ultra-High-Strength Concrete (UHSC, without fiber) are presented in **Table 1**. It is noted that there is no difference between the mix proportions of fresh water-mixed and seawater-mixed ones except for the water types. Type I ordinary Portland cement 52.5 N, silica fume with SiO_2 content over 92%, silica sand with an average particle size smaller than 300 μm, and polycarboxylate-based super-plasticizer (SP) were used in the matrix of UHS-ECC. The water-to-binder ratio was 0.20, the sand-to-binder ratio was 0.77, and the superplasticizer-to-binder ratio was 0.014. Ultra-high-molecular-weight PE fibers were used [60] [61] [62] and the fiber properties are listed in **Table 2**. The seawater was artificially produced by mixing tap water and dissolved commercial sea salt with a concentration of 36 g/L. The chemical composition of this artificial seawater type was confirmed to be similar to natural seawater in a previous study [63].

Table 1 Mix proportions (weight ratio).

Raw Materials	UHS-ECC	UHSC
Cement	1.000	1.000
Silica Fume	0.300	0.300
Silica Sand	1.000	1.000
Fresh Water (or Seawater)	0.260	0.260
Superplasticizer (in solid)	0.018	0.018
PE Fiber (Vol. %)	2.0%	0%

Table 2 Fiber properties (obtained from the suppliers).

Fiber Properties	Values
Diameter (μm)	24

Length (mm)	12
Strength (MPa)	3000
Modulus (GPa)	100
Density (g/cm^3)	0.97

The mixing process of UHS-ECC was as follows: (a) the cement, silica fume, and silica sand were dry-mixed for 2–3 min; (b) the water and superplasticizer were added into the mixer and stirred together for 6–8 min; (c) the PE fibers were added and mixed for another 3 min until a uniform mixture was formed; (d) the prepared mixture was cast into molds. All the specimens were cured in 23 ℃ water for 28 days.

2.2 FRP bars and grids

In this study, carbon FRP bars and grids were separately used as reinforcements (see **Fig. 2**). FRP grids were manufactured by Nippon Steel & Sumikin Materials Co., Ltd, Japan with a square mesh size of 50 mm × 50 mm. They are made up of untwisted yarns consisting of continuous carbon fibers impregnated with thermoset epoxy resin. According to the information provided by the manufacturer, the properties of the FRP bar/grid are as follows. The cross-sectional area of FRP grids (**Fig. 2a**) is 26.4 mm^2, and the tensile strength and elastic modulus of FRP grids were 1200 MPa and 165 GPa, respectively. The tensile strength and elastic modulus of 10 mm diameter FRP bars (**Fig. 2b**) are 1800 MPa and 120 GPa, respectively.

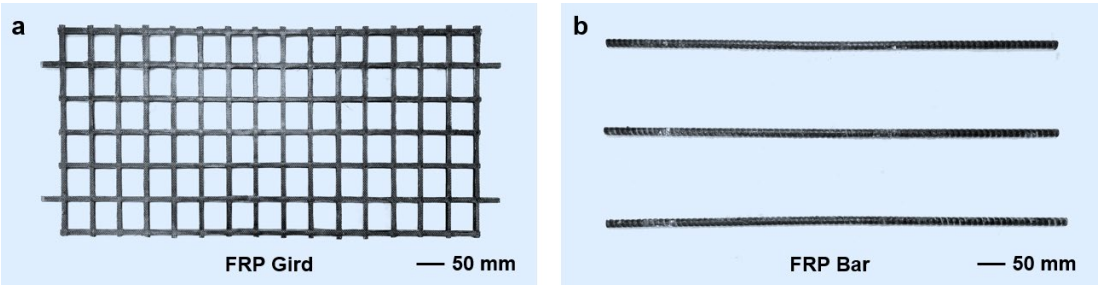

Fig. 2 Photographs of FRP reinforcements used: (a) FRP grids and (b) FRP bars.

127 *2.3 FRP-reinforced UHS-ECC panel*

128 A total of eight panels representing eight different groups were prepared for mechanical tests.
129 The specimen IDs are summarized in **Table 3**. Four panels were made of Ultra-High-Strength
130 Concrete (UHSC, without fiber) and the other four panels were prepared with UHS-ECC (2%
131 UHMWPE fiber). In the specimen IDs, "B" represents the FRP bar; "G" represents the FRP grid;
132 "SW" represents seawater; "FW" represents fresh water; and "0%" and "2%" stands for concrete
133 without fiber reinforcement (i.e., UHSC) and with 2% fiber reinforcement (i.e., UHS-ECC),
134 respectively. The panels had a length of 800 mm and a cross-section of 320 mm (width) × 50 mm
135 (depth). **Fig. 3** shows the details of the geometrical dimensions of FRP-reinforced UHS-ECC panels,
136 and both FRP bars and grids were placed at the bottom part of the panel with a cover thickness of 10
137 mm. It should be pointed out that based on the FRP reinforcements shown in **Fig. 2** and **Fig. 3**, the
138 total stiffness of the FRP bars used in the panel (120 GPa × 78.5 mm^2 × 3 = 28260 kN) was close to
139 that of the FRP grids (165 GPa × 26.4 mm^2 × 7 = 30492 kN).

140 **Table 3** Specimen IDs.

Specimen IDs	Types of Concrete (Fiber Volume Fraction)	Types of FRP Reinforcements	Types of Water
FW-B-0%	UHSC (**0%**)	Bar (**B**)	Fresh Water (**FW**)
SW-B-0%	UHSC (**0%**)	Bar (**B**)	Seawater (**SW**)
FW-G-0%	UHSC (**0%**)	Grid (**G**)	Fresh Water (**FW**)
SW-G-0%	UHSC (**0%**)	Grid (**G**)	Seawater (**SW**)
FW-B-2%	UHS-ECC (**2%**)	Bar (**B**)	Fresh Water (**FW**)
SW-B-2%	UHS-ECC (**2%**)	Bar (**B**)	Seawater (**SW**)
FW-G-2%	UHS-ECC (**2%**)	Grid (**G**)	Fresh Water (**FW**)
SW-G-2%	UHS-ECC (**2%**)	Grid (**G**)	Seawater (**SW**)

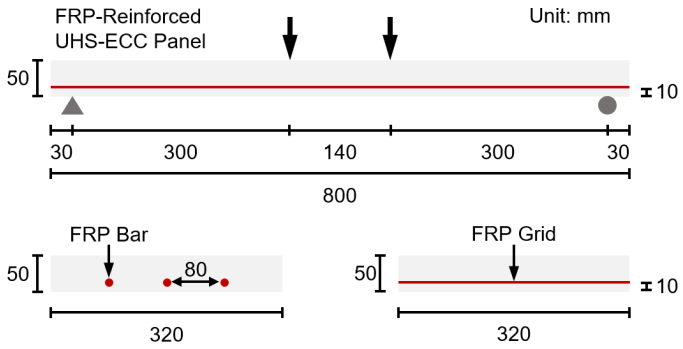

Fig. 3 Dimensions of FRP-reinforced UHS-ECC (UHSC) panels and test setup.

2.4 Testing methods and material properties

According to ASTM C469/C469M [64], the cube strength (50 mm × 50 mm × 50 mm cube) of fresh water-mixed UHS-ECC, seawater-mixed UHS-ECC, fresh water-mixed UHSC, and seawater-mixed UHSC were 150.4 MPa, 151.0 MPa, 150.9 MPa, and 150.6 MPa, respectively. It can be seen that the use of seawater and the addition of PE fibers had very limited effects on the cubic compressive strength. The compressive properties of UHS-ECC were further determined using Φ100 × 200 mm cylinders, according to the JSCE recommendation [65], and the measurement of elastic modulus also followed ASTM C469/C469M [64]. The average compressive strength and elastic modulus of fresh water-mixed UHS-ECC cylinders were 130.0 MPa (with the ultimate strain of 0.368%) and 38.0 GPa, respectively. For the seawater-mixed UHS-ECC cylinders, the average compressive strength and elastic modulus were 130.8 MPa (with the ultimate strain of 0.385%) and 38.2 GPa, respectively.

The direct tensile tests of UHS-ECC were conducted by using 13-mm thick dumbbell specimens (according to the JSCE's recommendation [65]) under the loading rate of 0.5 mm/min [66] [67] [68]. Linear variable differential transformers (LVDTs) were used to measure the tensile deformation of the central part (80-mm length) [69] [70]. The tensile stress-strain curves of UHS-ECC are presented in **Fig. 4**. From the figure, no obvious differences were observed in the tensile performances of these two types of UHS-ECC (i.e., FW-ECC and SW-ECC). Generally speaking, both UHS-ECC achieved

a tensile strain capacity of over 3.0% and a tensile strength of over 6.0 MPa showing significant tensile strain-hardening behaviors.

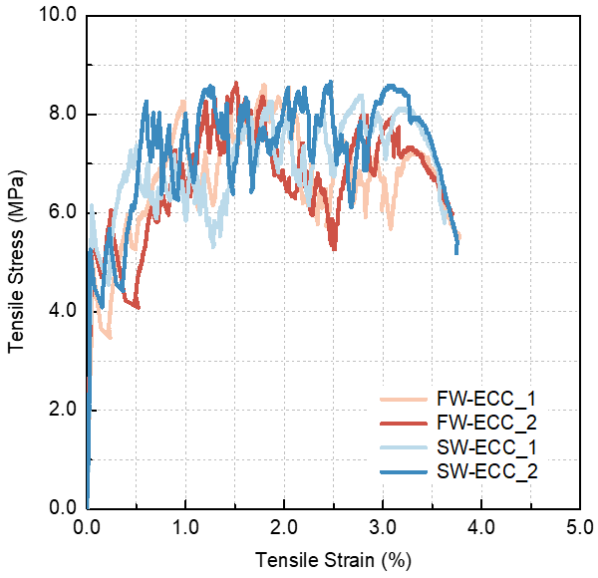

Fig. 4 Tensile stress-strain curves of UHS-ECC mixed with fresh water (FW-ECC) and seawater (SW-ECC). The use of seawater had a limited effect on the tensile behavior of UHS-ECC.

Four-point bending tests were carried out to evaluate the flexural behavior of FRP-reinforced UHS-ECC panels. The distance between the loading points was 140 mm, and the span was 740 mm. The specimens were tested using 150-kN hydraulic actuators under displacement control modes with a loading speed of 0.5 mm/min. A pair of LVDTs were used to measure the mid-span deflection of the specimens. Digital image correlation (DIC) method [71] [72] [73]was applied to analyze the tensile strain field and cracking behavior of FRP-reinforced UHS-ECC panels. The whole surface (800×50 mm^2) of the specimen was monitored using DIC, and the speckle pattern of black spots was applied onto the surface as a region of interest before the formal test. A digital camera was used to capture photographs at an interval of 3 s. For the DIC data processing, a subset size of 30 pixels and a step size of 15 pixels were chosen.

3 Test results and discussions

3.1 Flexural performance

The load-deflection curves of FRP-reinforced UHS-ECC (UHSC) panels are shown in **Fig. 5** and the values of load capacities are summarized in **Fig. 6**. The ultimate load and deflection of FRP bar-reinforced UHSC panel (FW-B-0% in **Fig. 5a**) were 19.7 kN and 9.4 mm, respectively, while those of FRP bar-reinforced UHS-ECC panel (FW-B-2% in **Fig. 5a**) increased by 173% (53.8 kN) and 167% (25.1 mm), respectively. For the FRP grid-reinforced UHS-ECC panel (FW-G-2% in **Fig. 5b**), the load capacity and deflection were 62.5 kN and 19.6 mm, respectively, which were 139% and 54% larger than those of UHSC panels (FW-G-0%, 26.2 kN and 12.7 mm), respectively. As summarized in **Fig. 5c**, compared with the FRP-reinforced UHSC panel, the load capacity and stiffness of the FRP-reinforced UHS-ECC panel significantly increased. It should be pointed out that in accordance with the Chinese Standard GB 50666-2011 [74], the flexural capacity of the developed FRP bar-reinforced UHS-ECC panel was found to exceed the required capacity for a one-meter-high cast-in-site concrete by over 20 times. In future studies, the FRP-reinforced UHS-ECC panel can be further designed as a formwork panel, and the loading scheme needs be determined based on the shape and size of the concrete member produced by the designed formwork.

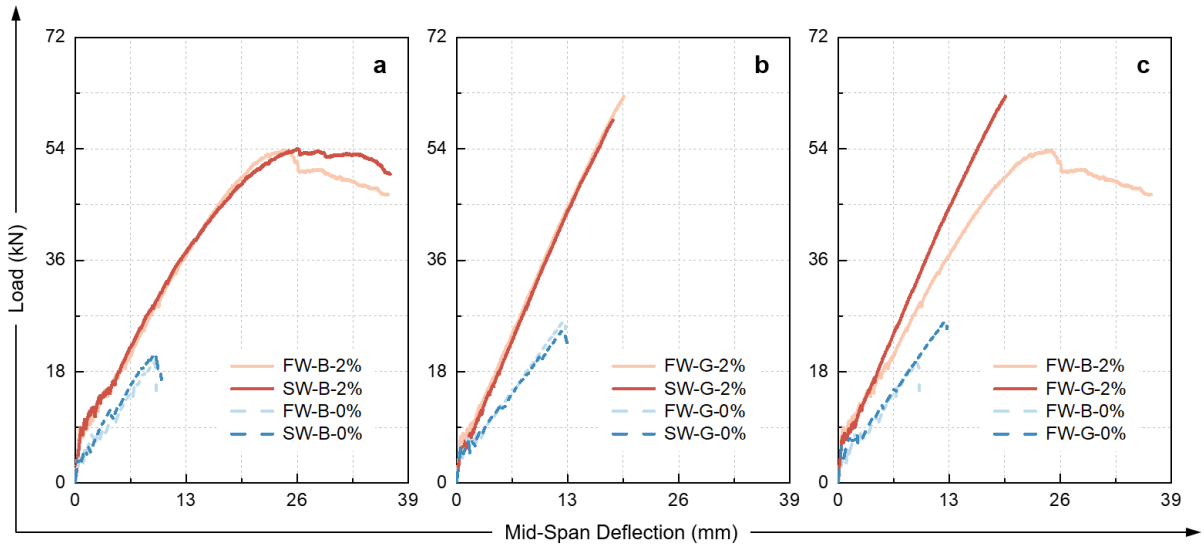

Fig. 5 Load-deflection curves of FRP-reinforced UHS-ECC (UHSC) panels. The flexural performance of the FRP-reinforced UHS-ECC panel showed significantly higher load capacity and stiffness than the FRP-UHSC counterpart, and the use of seawater had a limited effect on the flexural behavior.

Fig. 5a and **Fig. 5b** also show the load-deflection curves of FRP-reinforced panels using seawater. In general, the use of seawater as raw material had no obvious effect on the flexural performance of FRP-reinforced UHS-ECC (UHSC) panels. This phenomenon can be explained as follows: seawater had a negligible effect on the compressive and tensile performance of UHSC and UHS-ECC (as presented in ***Section 2.4***), which was also reported in many papers [63] [75].

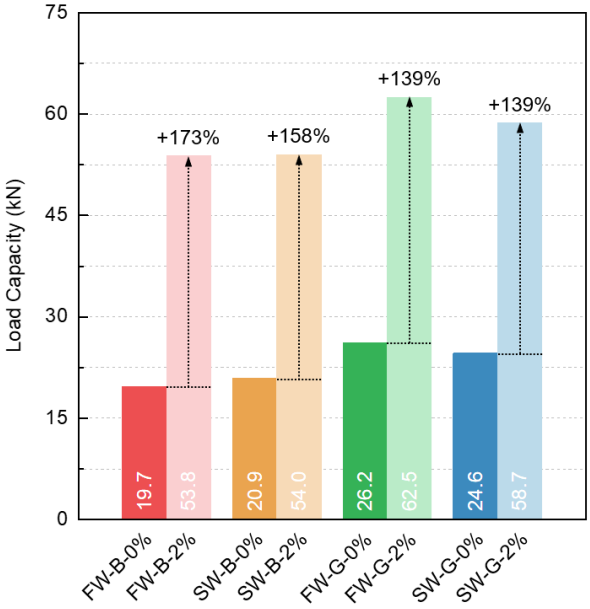

Fig. 6 Load capacities of FRP-reinforced UHS-ECC/UHSC panels. The FRP-reinforced UHS-ECC panel showed 139%–173% higher load capacity than the FRP-UHSC counterpart.

Fig. 7 shows the crack patterns of FRP-reinforced UHS-ECC (UHSC) panels at the ultimate stage. During the tests, shear failure occurred in all the UHSC panels (without PE fibers), the compression failure of UHS-ECC occurred in FW-B-2% and SW-B-2% with multiple narrowed cracks along the panel span, and the rupture of the FRP grid occurred in FW-G-2% and SW-G-2%. Compared to FW-B-2%, much fewer cracks were observed in FW-B-0%, showing that adding PE fibers can significantly improve the energy absorption and ductility of the structural members. **Fig. 8** presents the photographs of FW-B-0% and FW-B-2% after bending tests. It can be seen that the UHSC panel broke into pieces and cracks occurred along the FRP bars (**Fig. 8a**), while the integrity of the UHS-ECC panel is good (**Fig. 8b**). It is noted that the abrupt drop of load-bearing capacity in FRP grid-reinforced UHS-ECC panels (**Fig. 5b**) was caused by the rupture of FRP grid, indicating that UHS-ECC and FRP grid had good deformation compatibility and interaction.

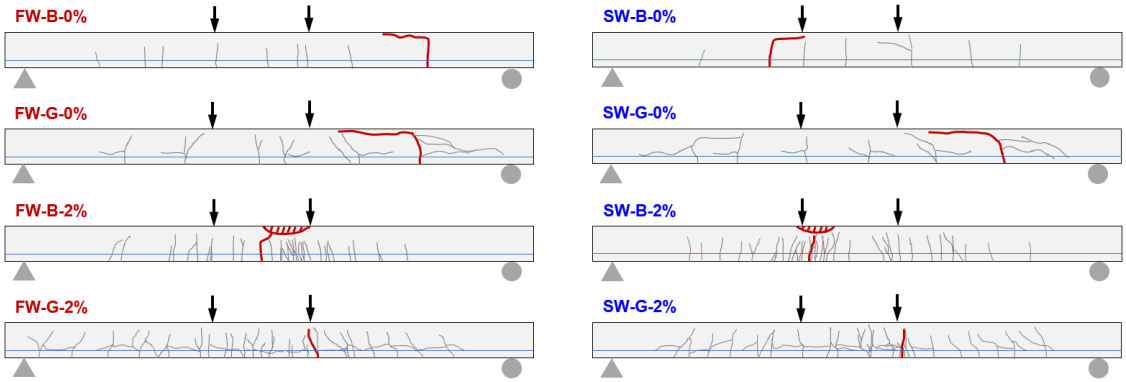

Fig. 7 Crack patterns of FRP-reinforced UHS-ECC (UHSC) panels at the ultimate stage. For UHS-ECC and UHSC panels, flexural and shear failure occurred, respectively.

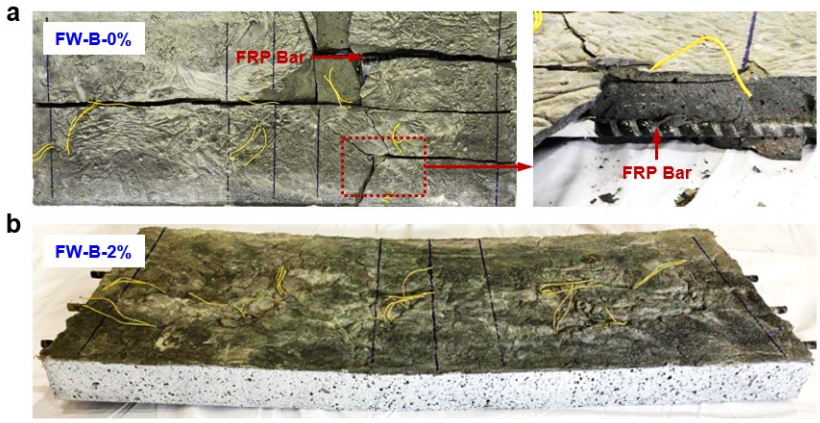

Fig. 8 Photographs of (a) UHS-ECC (FW-B-0%) and (b) UHSC (FW-B-2%) panels after bending tests. The integrity of the UHS-ECC panel is good, but the UHSC panel broke into pieces.

A comparison between the load-deflection curves of FRP bar- and grid-reinforced panels is presented in **Fig. 5c**. The flexural capacities of FW-G-2% and FW-G-0% were 16% and 33% higher than that of FW-B-2% and FW-B-0%, respectively. In FRP grid-reinforced UHS-ECC panels, the UHS-ECC passing through the openings of the FRP grid worked as "shear keys", and the interaction between the FRP grid and UHS-ECC could transfer stresses in the longitudinal FRP strips to the UHS-ECC through the transverse strips. Also, the cracks of FRP grid-reinforced panels were more evenly distributed than those of FRP bar-reinforced ones (**Fig. 7**). It should be remembered that the total stiffness of FRP bars and grids used in the panels was close, leading to the similar stiffness of FW-G-

0% and FW-B-0% as shown in **Fig. 5c**. For FW/SW-G-2% in **Fig. 5b**, the panel stiffness remained almost unchanged after cracking load. However, for FW/SW-B-2% in **Fig. 5a**, the panel stiffness decreased as the load approached the peak value, indicating that the debonding of FRP bars occurred.

3.2 Strain profiles

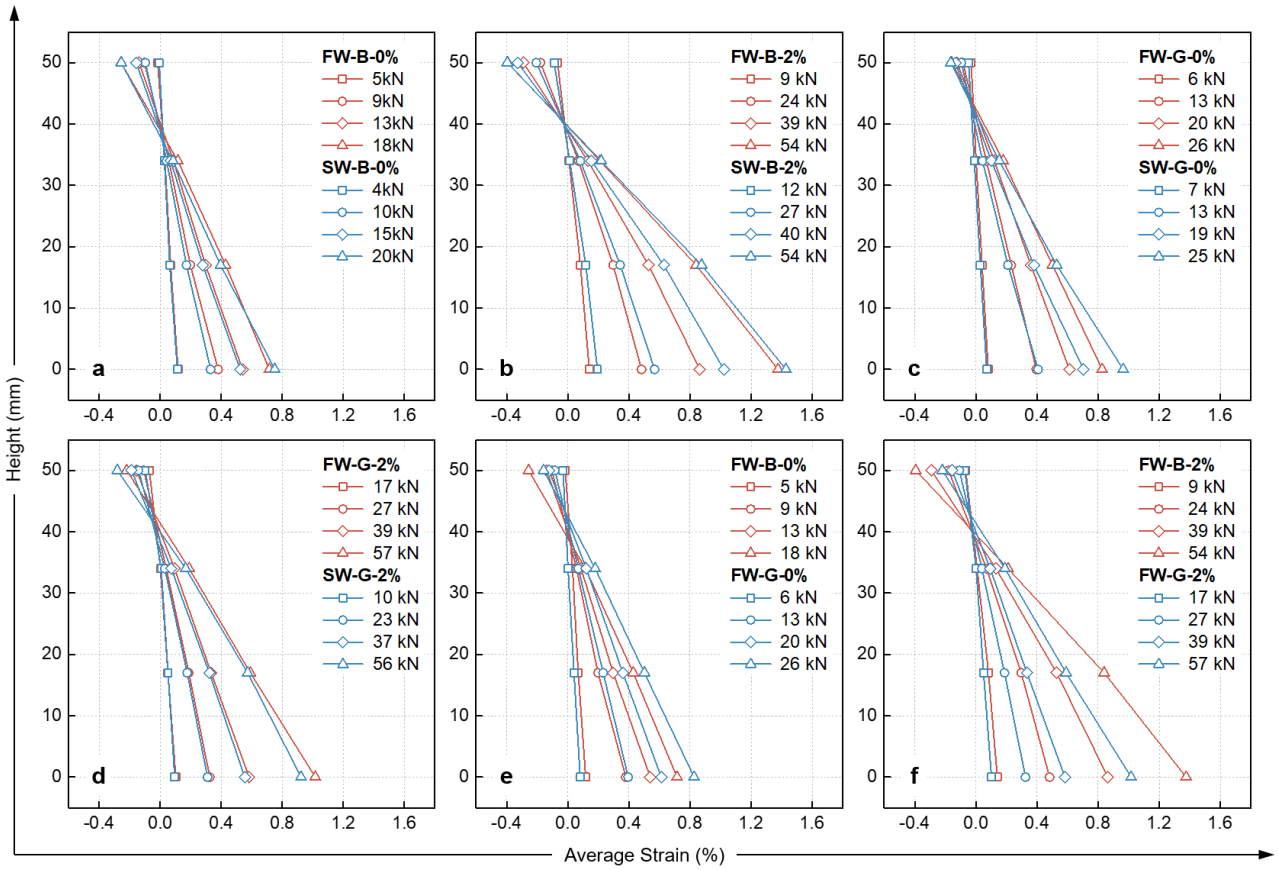

Fig. 9 The strain profiles of FRP-reinforced UHS-ECC/UHSC panels almost remained a linear variation, indicating that the plane section could be assumed in the sectional analysis of the panels.

The strain profiles of panels at four different load levels are summarized in **Fig. 9**. It is noted that the results in **Fig. 9** were obtained from DIC analysis following the method in Ref. [76]. It is seen that during the loading process, all the strain profiles were linearly distributed along the section height, indicating that the plane section assumption could be adopted in sectional analysis (***Section 5***). In **Fig. 9a–d,** the strain profiles of seawater-mixed specimens were close to those of fresh water-mixed ones, which was in accordance with the results that using seawater had almost no effect on the flexural

behavior of the FRP-reinforced panels. The comparison under the similar load level between FRP bar- and grid-reinforced panels is shown in **Fig. 9f**. The strains of FRP grid-reinforced UHS-ECC panels were smaller than those of FRP bar-reinforced UHS-ECC panels at high load levels, due to the reduction of the panel stiffness of FW-B-2% caused by the debonding of FRP bars.

3.3 Evolution of the maximum crack width

The maximum crack width *vs.* load relations of the FRP-reinforced panels (**Fig. 10**) were measured by DIC techniques according to the method in Ref. [76]. Compared with the UHSC panels, the addition of PE fibers in UHS-ECC reduced the maximum crack width significantly due to the fiber-bridging effect. In **Fig. 10**, it can be seen that when the load level was over 10 kN, the FRP grid-reinforced UHS-ECC panels (i.e., FW/SW-G-2%) possessed a better crack control ability than FRP bar-reinforced UHS-ECC panels (i.e., FW/SW-B-2%), which could be attributed to the stronger bond interaction between FRP grid and UHS-ECC.

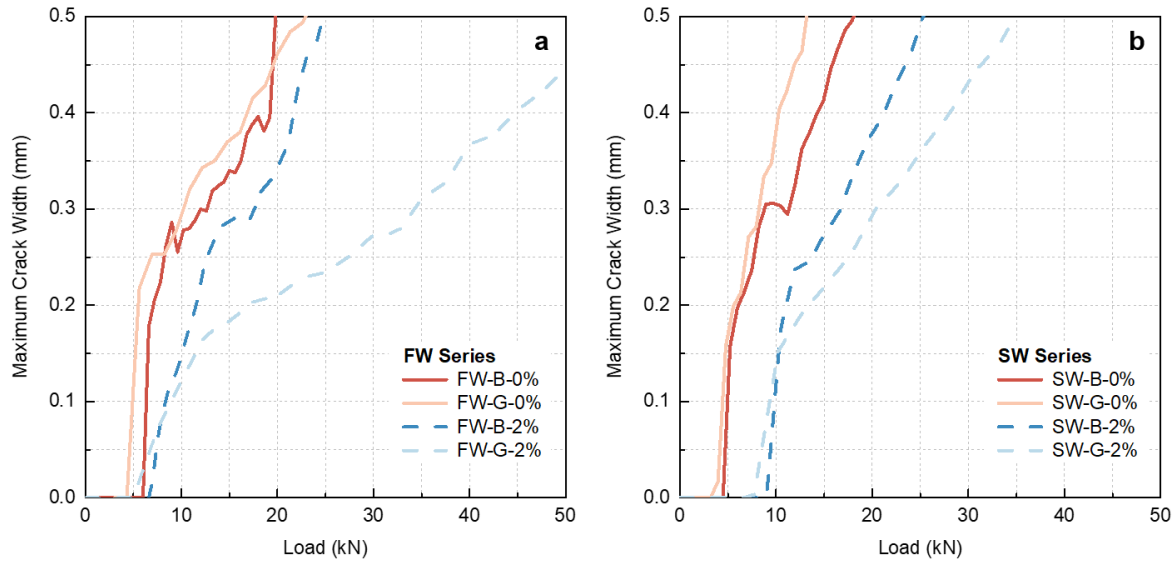

Fig. 10 Evolution of the maximum crack width of FRP-reinforced panel: (a) Freshwater (FW) series and (b) seawater (SW) series. Using UHS-ECC to replace UHSC significantly enhanced the crack resistance of the FRP-reinforced panel.

4 DIC analysis and failure process

4.1 FRP bar/grid-reinforced UHSC (without fiber)

Fig. 11 and **Fig. 12** show the failure processes of FRP bar/grid-reinforced panels using fresh water/seawater-mixed UHSC. The DIC results at four load levels (i.e., 0.25P_u, 0.50P_u, 0.75P_u, 1.00P_u, P_u is the peak load) are compared. At the load level of 0.25P_u, several cracks were initiated at the panel bottom. Then, the crack number increased with the increasing load. At the ultimate load, the tip of the major crack was very close to the top side of the member, and the shear failures occurred at both FRP bar- and grid-reinforced UHSC panels (see also **Fig. 7**). The load capacity of FW-G-0% was 16% higher than that of FW-B-0%, indicating a better interaction between UHSC and FRP grids. It should be noted that transverse cracks in the FRP grid-reinforced panels propagated along the longitudinal direction of panels, which is possibly due to the stress concentration occurring at the grid knots.

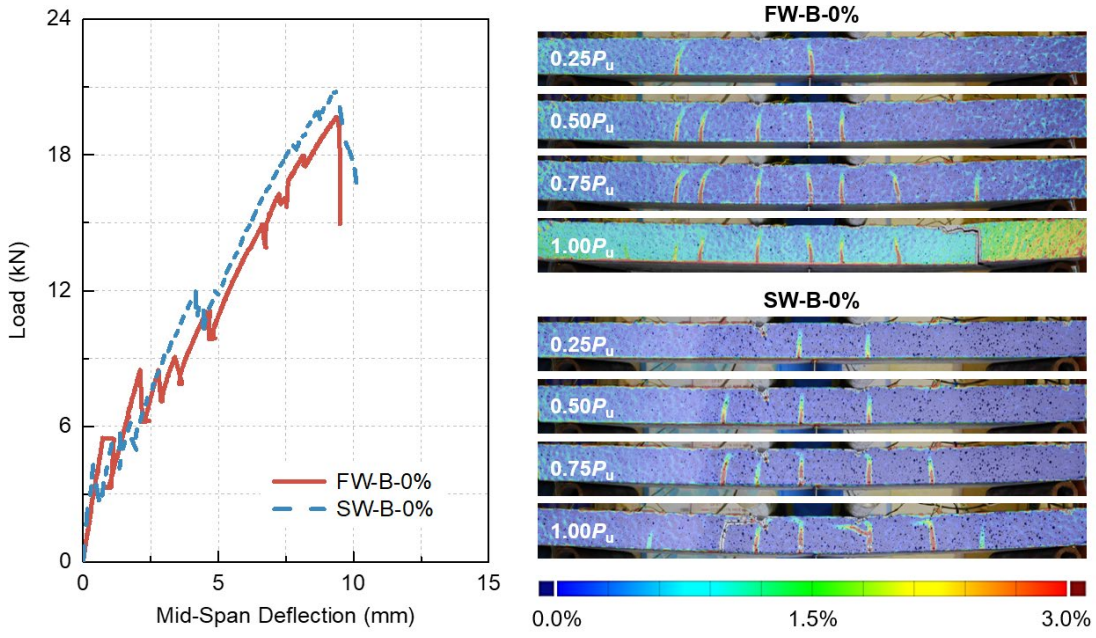

Fig. 11 Failure processes of FRP bar-reinforced panels using fresh water and seawater-mixed UHSC.

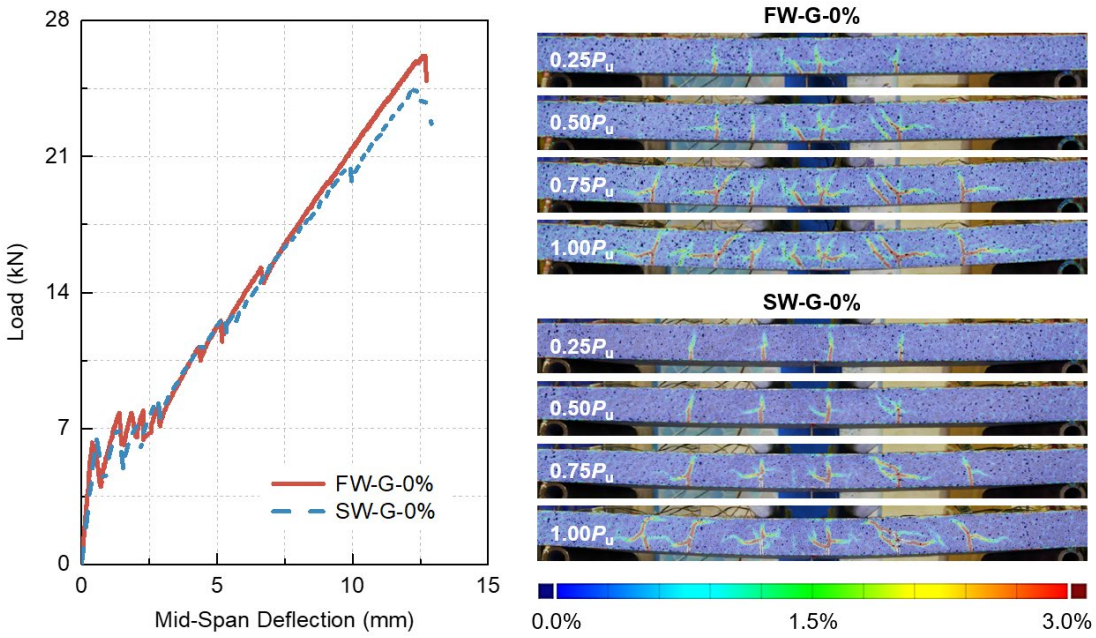

Fig. 12 Failure processes of FRP grid-reinforced panels using fresh water and seawater-mixed UHSC.

4.2 FRP bar/grid-reinforced UHS-ECC (2% PE fibers)

The failure processes of FW/SW-B-2% and FW/SW-G-2% are presented in **Fig. 13** and **Fig. 14**, respectively. At the load level of 0.25P_u, more cracks were observed in FRP-reinforced UHS-ECC panels, compared to FRP-reinforced UHSC panels in **Fig. 11** and **Fig. 12**. The crack number of all the panels increased with the increasing load level. Different from the FRP-UHSC panels, the shear failure did not occur in UHS-ECC panels. Instead, flexural failure occurred in all the UHS-ECC specimens. The compressive failure of UHS-ECC was observed at FW/SW-B-2% (see also **Fig. 7**), and the debonding of FRP bars led to a more ductile failure mode after the ultimate load than FW/SW-G-2% in **Fig. 14**. For the FRP grid-reinforced UHS-ECC panel, multiple vertical cracks initiated from the bottom of the panel and started to turn into transverse cracks when they approached the grid knots (**Fig. 14**). Finally, the tip of the major crack almost reached the top of the panel, but the crushing failure of concrete did not occur. Instead, the failure of FW/SW-G-2% was governed by the rupture of FRP grids, indicating that this system took full advantage of the tensile strength of FRP material.

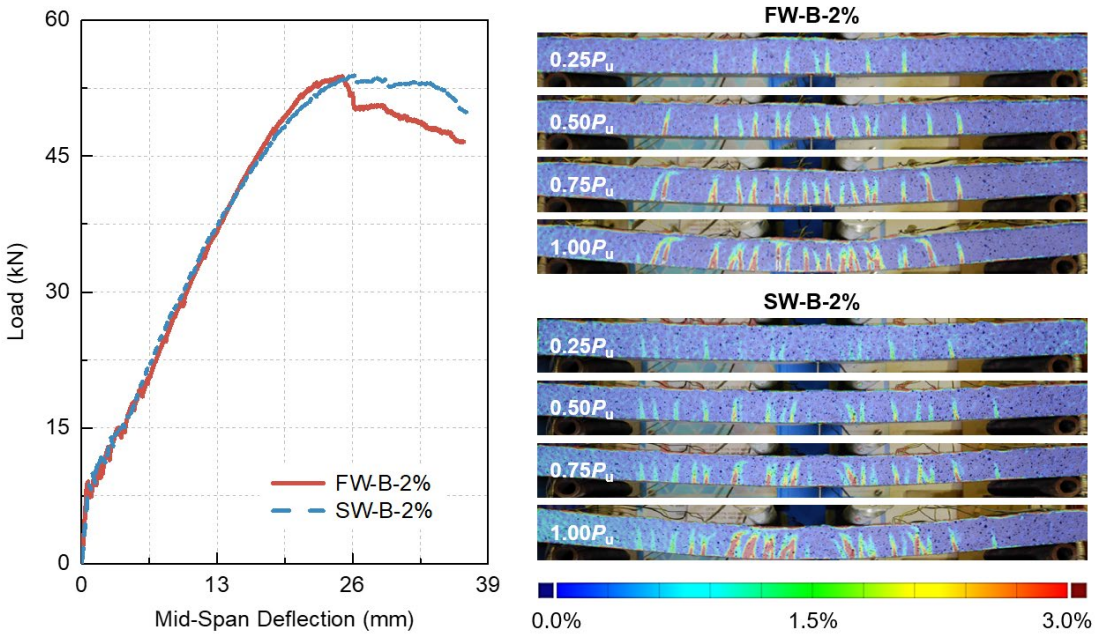

Fig. 13 Failure processes of FRP bar-reinforced panels using fresh water and seawater-mixed UHS-ECC.

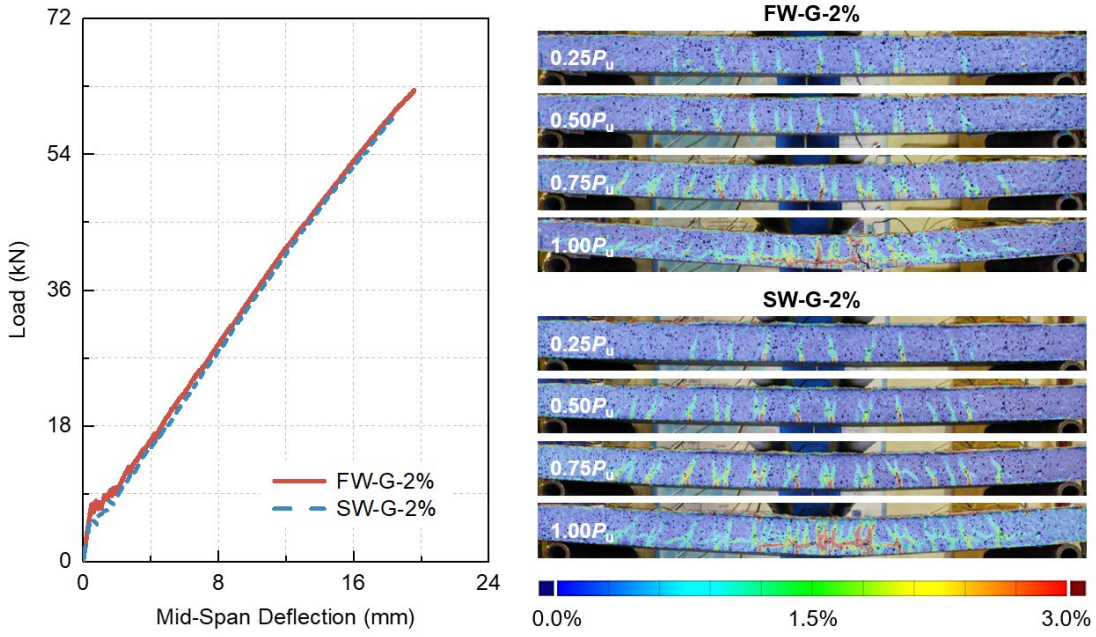

Fig. 14 Failure processes of FRP grid-reinforced panels using fresh water and seawater-mixed UHS-ECC.

For the FRP grid-reinforced UHS-ECC panel, the tensile strength of the FRP grid can be used to determine the stress level at the ultimate load, because the rupture failure of the FRP grid occurred (i.e., the strength of the FRP gird was fully utilized). For the FRP bar-reinforced UHS-ECC panel, the

actual stress level remained unknown, because the debonding of the FRP bar occurred and the rupture failure of the FRP bar was not observed. In future studies, the local tensile strain of the FRP bar/grid can be measured by strain gauges or optical fibers to calculate the actual stress level.

4.3 Composites action of FRP reinforcement and UHS-ECC

Considering that strong stress concentration and large crack width are difficult to avoid in conventional FRP bar/grid-reinforced concrete structures (**Fig. 15**), the replacement of conventional concrete with UHS-ECC can be an effective way to overcome the above drawbacks. As UHS-ECC possesses excellent mechanical properties, superior tensile ductility, and multiple cracking behavior, the deformation compatibility between FRP and UHS-ECC was much better than that between FRP and concrete (**Fig. 15**). In detail, under flexural (**Fig. 15a**) or shear (**Fig. 15b**) loadings, the cracking of conventional concrete (i.e., comparatively large cracks) results in a strong interfacial shear stress concentration along FRP reinforcement, while the multiple cracking behavior of UHS-ECC (i.e., multiple fine cracks) can effectively lower such stress concentration, leading to a better composite action between UHS-ECC and FRP. It means that the strain localization in the FRP bar/grid could be effectively alleviated, but could not be avoided in UHS-ECC, owing to the existence of the multiple fine cracks. According to the experimental results and the composite action revealed in this study, the combination of FRP reinforcement and UHS-ECC is proved to have excellent mechanical performance, showing great potential in the applications of marine and coastal structures. It should be remembered that for FRP-reinforced ECC systems in marine and coastal construction, seawater and sea-sand can be used in ECC to improve material sustainability, as FRP reinforcement is non-corrosive.

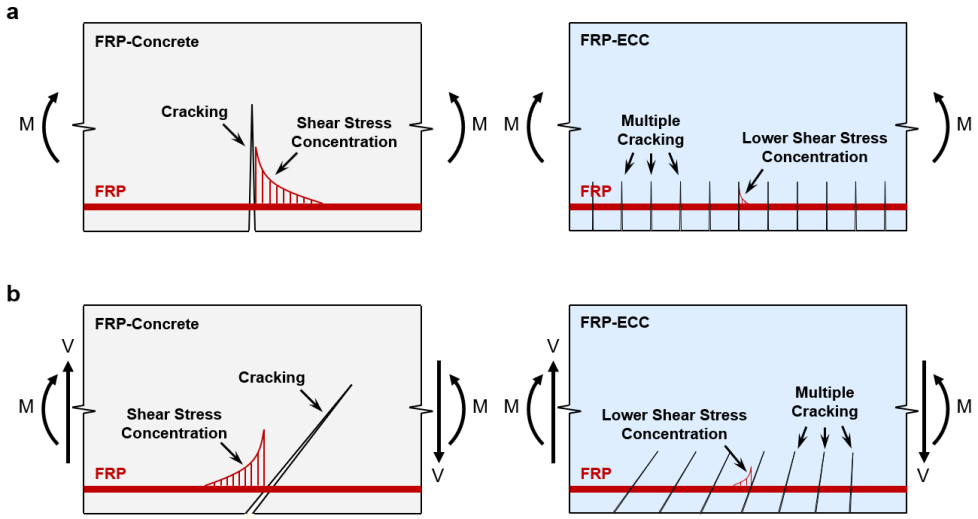

Fig. 15 Influence of cracking behavior on the interfacial stress of FRP bar/grid-reinforced panel.

The multiple cracking behavior of ECC materials lowered the crack-induced shear stress concentration along the FRP reinforcement.

5 Theoretical analysis

5.1 Calculation of load capacity

Based on the stress and strain distribution shown in **Fig. 16**, sectional analysis was conducted to calculate the ultimate loads of the FRP-reinforced UHS-ECC panels. Here, b and h are the width and height of the section, respectively; m is the location of the FRP reinforcement; c is the location of the neutral axis; ε_c, ε_f, and ε_t are the strains of UHS-ECC in compression zone, FRP in tension zone, and UHS-ECC in tension zone, respectively; σ_c and σ_t are the stresses of UHS-ECC in compression and tension, respectively; and ε_{cu} is the ultimate compressive strain of UHS-ECC, respectively. The tensile force of the panel was determined by combining the tensile contribution provided by both FRP reinforcement and UHS-ECC. It is noted that the UHS-ECC crushing failure occurred in FRP bar-reinforced UHS-ECC panels, while the FRP rupture occurred in FRP gird-reinforced UHS-ECC panels. Thus, two different ultimate conditions were applied to estimate the load capacities.

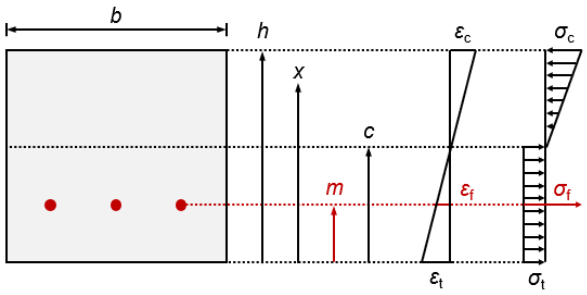

Fig. 16 Stress and strain distributions of FRP-reinforced UHS-ECC panel at the ultimate stage.

For UHS-ECC, the compressive stress-strain relationship recommended by the specification of the Japan Society of Civil Engineers (JSCE) [77] was used.

$$\sigma_c = \begin{cases} E_c\varepsilon & \left(0 \le \varepsilon \le \varepsilon_{ce}\right) \\ f_c & \left(\varepsilon_{ce} < \varepsilon \le \varepsilon_{cu}\right) \end{cases} \quad \textbf{(1)}$$

where E_c and f_c are the measured elastic modulus (38.0 GPa) and compressive strength (130.0 MPa), respectively; ε_{ce} and ε_{cu} are 0.342% and 0.368%, respectively.

For the sectional analysis, the tensile behavior of the FRP reinforcement was assumed to be linear elastic, the material properties can be found in ***Section 2***. The equilibrium equations of the conditions in **Fig. 16** can be expressed as follows:

$$\sum N = 0 \Rightarrow \int_c^h \sigma_c b dx = E_f \varepsilon_f A_f + \int_0^c \sigma_t b dx \quad \textbf{(2)}$$

$$\sum M = 0 \Rightarrow M_{\text{Calcu}} = \int_c^h \sigma_c \left(x - c\right) b dx + E_f \varepsilon_f A_f \left(c - m\right) + \int_0^c \sigma_t \left(c - x\right) b dx \quad \textbf{(3)}$$

where A_f is the total area of FRP reinforcement in the tension zone; E_f is the elastic modulus of FRP reinforcement. For FRP bar-reinforced UHS-ECC at the ultimate load, the strain of UHS-ECC at the top of the panel was set to ε_{cu} (0.368%), because the compressive failure of UHS-ECC occurred. For FRP grid-reinforced UHS-ECC at the ultimate load, the rupture of FRP grids occurred, and thus the strain of FRP in tension was set to the rupture strain ε_{fu} (0.73%). The tensile strength and strain capacity of UHS-ECC were assumed to be 6.0 MPa and 3.0%, respectively.

As shear failure occurred in all the UHSC panels (**Fig. 7**), the load capacities of FW/SW-B-0% and FW/SW-G-0% were contributed by the shear force of UHSC (V_c), and the contribution of longitudinal FRP reinforcement was neglected. The shear capacities of FRP-reinforced UHSC panels can be estimated based on the equation given in ACI318M-14 [78]:

$$V_c = (0.16\lambda\sqrt{f_c} + 17\rho\frac{d}{a})bd \quad \textbf{(4)}$$

where λ is a modification factor (taken as 1.0 here); ρ is the longitudinal reinforcement ratio; a and d are the length of the shear span (300.0 mm) and effective depth (40.0 mm) of the panel, respectively.

Based on **Eq. (2)**, **Eq. (3)**, and **Eq. (4)**, the ultimate load capacities of FRP-reinforced UHS-ECC and FRP-reinforced UHSC panels can be calculated and the results are summarized in **Table 4**. The comparison of the experimental and predicted results is shown in **Fig. 17**. In general, the prediction error was acceptable with a maximum variation of around 20%. It can be found in **Table 4** that all the calculated load capacities of FRP grid-reinforced panels (i.e., FW-G-0%, SW-G-0%, FW-G-2%, and SW-G-2%) showed smaller prediction errors than those of FRP bar-reinforced panels (i.e., FW-B-0%, SW-B-0%, FW-B-2%, and SW-B-2%). This phenomenon is related to the fact that FRP grids showed better interaction with UHS-ECC (UHSC) than FRP bars and the debonding of FRP bars occurred during the tests. It should be noted that as only one specimen of each group was adopted in this work, the test results were not enough to provide a reliable structural design recommendation. In the future study, additional experimental results are needed to propose a design method for FRP bar/grid-reinforced UHS-ECC panels.

Table 4 Test and calculated load capacities of FRP-reinforced panels.

Specimen IDs	Ultimate Load (kN)		
	Test (kN)	Calculation (kN)	Variation (%)
FW-B-0%	19.7	23.8	+20.8

SW-B-0%	20.9	23.8	+13.9
FW-G-0%	26.2	23.7	-9.5
SW-G-0%	24.6	23.7	-3.7
FW-B-2%	53.8	64.5	+19.9
SW-B-2%	54	64.5	+19.4
FW-G-2%	62.5	64.2	+2.7
SW-G-2%	58.7	64.2	+9.4

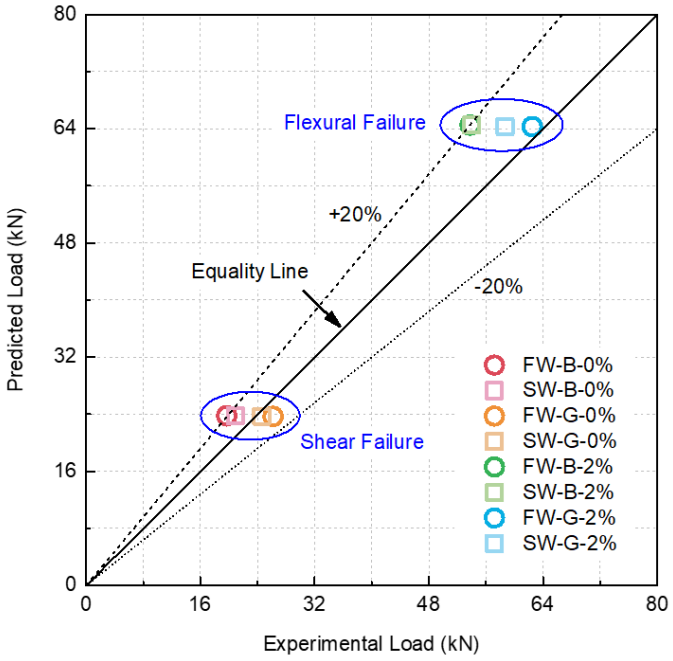

Fig. 17 Comparison of test and calculated load capacities. The prediction error was acceptable with the maximum variation around 20%.

6 Conclusions

In this study, a novel Ultra-High-Strength Engineered Cementitious Composites (UHS-ECC) panel with Fiber-Reinforced Polymer (FRP) reinforcement (i.e., FRP bar or grid) was proposed for the construction of sustainable marine structures. The flexural performance and composite action of FRP-reinforced UHS-ECC panels were experimentally and analytically investigated. The findings can be summarized as follows.

- In the four-point bending test, the flexural failure occurred in the FRP-reinforced UHS-ECC panels, while the shear failure occurred in the FRP-reinforced Ultra-High-Strength Concrete (UHSC, without fibers) panels. Compared with the FRP-reinforced UHSC panel, the FRP-reinforced UHS-ECC panel showed significantly higher ultimate load (139%–173% higher), stiffness, and deformation capacity. It was also found that the use of seawater had almost no effect on the mechanical performance of FRP-reinforced UHS-ECC (UHSC) panels.

- The results showed that the combination of FRP grid and UHS-ECC had the potential to take full advantage of the tensile strength of FRP material. Compared with the FRP gird-reinforced UHS-ECC panel, the use of FRP bars lowered the stiffness and load capacity of the panel owing to the debonding of FRP bars in UHS-ECC.

- An analytical investigation was conducted to predict the load capacities of the tested panels. In general, the calculated ultimate loads of FRP grid-reinforced panels showed better agreement with the experimental results than FRP bar-reinforced panels.

- It was revealed that using UHS-ECC to replace UHSC improved the stress transfer and deformation compatibility with FRP because the multiple cracking behavior of UHS-ECC lowered the crack-induced shear stress concentration along the FRP reinforcement.

This study provides the first trial of the combined use of UHS-ECC and FRP reinforcement in structural members, and the results demonstrated the feasibility of this novel system. It should be pointed out that the developed FRP-reinforced UHS-ECC system can be used for stay-in-place permanent formwork, high-performance strengthening layer, and thin-wall structural members (e.g., tubular column and box beam). Currently, an experimental investigation is being carried out by the authors to use FRP-reinforced UHS-ECC as the stay-in-place permanent formwork and strengthening

layer for reinforced concrete structures, and the results will be reported in the future. In addition, the durability performance of this novel system is suggested to be systematically investigated.

Acknowledgments

This study was supported by the Innovation Technology Fund of the Hong Kong Government (No. ITS/077/18FX) and R&D Project of China Overseas Holdings Limited (No. COHL-2021-Z-1-03). Ji-Xiang Zhu and Ke-Fan Weng acknowledge the PhD studentship offered by The Hong Kong Polytechnic University. Bo-Tao Huang would like to acknowledge the support of the National Natural Science Foundation of China (Nos. 52308290 and 52338003) and the National Natural Science Fund for Excellent Young Scientists Fund Program (Overseas).

CRediT Author Statement

JX Zhu: Conceptualization, Methodology, Investigation, Validation, Data Curation, Writing - Original Draft. **KF Weng**: Investigation, Validation, Formal analysis. **BT Huang**: Conceptualization, Methodology, Visualization, Writing - Review & Editing. **LY Xu**: Data Curation, Writing - Review & Editing. **JG Dai**: Funding Acquisition, Supervision, Writing - Review & Editing.

References

[1] Zhang, C., Wu, L., Elchalakani, M., & Cai, J. (2023). Cyclic loading test for reinforced concrete columns strengthened with high-strength engineered cementitious composite jacket. Engineering Structures, 278, 115571.

[2] Cai, J., Pan, J., Tan, J., & Li, X. (2020). Bond behaviours of deformed steel rebars in engineered cementitious composites (ECC) and concrete. Construction and Building Materials, 252, 119082.

[3] Cai, J., Pan, J., Xu, L., Li, G., & Ma, T. (2021). Mechanical behavior of RC and ECC/RC composite frames

under reversed cyclic loading. Journal of Building Engineering, 35, 102036.

[4] Xu, L., Pan, J., & Cai, J. (2019). Seismic performance of precast RC and RC/ECC composite columns with grouted sleeve connections. Engineering Structures, 188, 104-110.

[5] Huang, B. T., Yu, J., Wu, J. Q., Dai, J. G., & Leung, C. K. (2020). Seawater sea-sand Engineered Cementitious Composites (SS-ECC) for marine and coastal applications. Composites Communications, 20, 100353.

[6] Neville, A. (2004). The confused world of sulfate attack on concrete. Cement and Concrete Research, 34(8), 1275-1296.

[7] Zhang, K., Zhang, Q., & Xiao, J. (2022). Durability of FRP bars and FRP bar reinforced seawater sea sand concrete structures in marine environments. Construction and Building Materials, 350, 128898.

[8] Yi, Y., Zhu, D., Guo, S., Zhang, Z., & Shi, C. (2020). A review on the deterioration and approaches to enhance the durability of concrete in the marine environment. Cement and Concrete Composites, 113, 103695.

[9] Pech-Canul, M. A., & Castro, P. (2002). Corrosion measurements of steel reinforcement in concrete exposed to a tropical marine atmosphere. Cement and Concrete Research, 32(3), 491-498.

[10] Huang, B. T., Li, Q. H., Xu, S. L., & Zhou, B. M. (2018). Tensile fatigue behavior of fiber-reinforced cementitious material with high ductility: Experimental study and novel PSN model. Construction and Building Materials, 178, 349-359.

[11] Huang, B. T., Li, Q. H., & Xu, S. L. (2019). Fatigue deformation model of plain and fiber-reinforced concrete based on Weibull function. Journal of Structural Engineering, 145(1), 04018234.

[12] Cui, W., Wang, F., & Huang, X. (2011). A unified fatigue life prediction method for marine structures. Marine Structures, 24(2), 153-181.

[13] Dong, Y., Garbatov, Y., & Soares, C. G. (2022). Review on uncertainties in fatigue loads and fatigue life of ships and offshore structures. Ocean Engineering, 264, 112514.

443 [14] Jimenez-Martinez, M. (2020). Fatigue of offshore structures: A review of statistical fatigue damage assessment
444 for stochastic loadings. International Journal of Fatigue, 132, 105327.

445 [15] Lin, G., & Teng, J. G. (2020). Advanced stress-strain model for FRP-confined concrete in square columns.
446 Composites Part B: Engineering, 197, 108149.

447 [16] Lin, G., Zeng, J. J., Teng, J. G., & Li, L. J. (2020). Behavior of large-scale FRP-confined rectangular RC
448 columns under eccentric compression. Engineering Structures, 216, 110759.

449 [17] Peng, K. D., Huang, B. T., Xu, L. Y., Hu, R. L., & Dai, J. G. (2022). Flexural strengthening of reinforced
450 concrete beams using geopolymer-bonded small-diameter CFRP bars. Engineering Structures, 256, 113992.

451 [18] Meng, W., Khayat, K. H., & Bao, Y. (2018). Flexural behaviors of fiber-reinforced polymer fabric reinforced
452 ultra-high-performance concrete panels. Cement and Concrete Composites, 93, 43-53.

453 [19] Ye, Y. Y., Smith, S. T., Zeng, J. J., Zhuge, Y., & Quach, W. M. (2021). Novel ultra-high-performance concrete
454 composite plates reinforced with FRP grid: Development and mechanical behaviour. Composite Structures,
455 269, 114033.

456 [20] Liu, W. W., Ouyang, L. J., Gao, W. Y., Liang, J., Wang, T. C., Song, J., & Yang, J. (2023). Repair of fire-
457 damaged RC square columns with CFRP textile-reinforced ECC matrix. Engineering Structures, 292, 116530.

458 [21] Benmokrane, B., Sanni Bakouregui, A., Mohamed, H. M., Thébeau, D., & Abdelkarim, O. I. (2020). Design,
459 construction, and performance of continuously reinforced concrete pavement reinforced with GFRP bars: Case
460 study. Journal of Composites for Construction, 24(5), 05020004.

461 [22] Kara, I. F., Ashour, A. F., & Dundar, C. (2013). Deflection of concrete structures reinforced with FRP bars.
462 Composites Part B: Engineering, 44(1), 375-384.

463 [23] Barris, C., Torres, L., Vilanova, I., Mias, C., & Llorens, M. (2017). Experimental study on crack width and
464 crack spacing for Glass-FRP reinforced concrete beams. Engineering structures, 131, 231-242.

[24] Lau, D., & Pam, H. J. (2010). Experimental study of hybrid FRP reinforced concrete beams. Engineering Structures, 32(12), 3857-3865.

[25] Arduini, M., Di Tommaso, A., & Nanni, A. (1997). Brittle failure in FRP plate and sheet bonded beams. ACI Structural Journal, 94(4), 363-370.

[26] Camata, G., Spacone, E., & Zarnic, R. (2007). Experimental and nonlinear finite element studies of RC beams strengthened with FRP plates. Composites Part B: Engineering, 38(2), 277-288.

[27] Li, V. C. (2019). Engineered Cementitious Composites (ECC) - Bendable Concrete for Sustainable and Resilient Infrastructure. Verlag GmbH Germany: Springer, Berlin, Heidelberg.

[28] Ding, Y., Yu, K., & Li, M. (2022). A review on high-strength engineered cementitious composites (HS-ECC): Design, mechanical property and structural application. Structures, 35, 903-921.

[29] Yu, K., McGee, W., Ng, T. Y., Zhu, H., & Li, V. C. (2021). 3D-printable engineered cementitious composites (3DP-ECC): Fresh and hardened properties. Cement and Concrete Research, 143, 106388.

[30] Yu, K. Q., Zhu, W. J., Ding, Y., Lu, Z. D., Yu, J. T., & Xiao, J. Z. (2019). Micro-structural and mechanical properties of ultra-high performance engineered cementitious composites (UHP-ECC) incorporation of recycled fine powder (RFP). Cement and Concrete Research, 124, 105813.

[31] Yu, K., Li, L., Yu, J., Wang, Y., Ye, J., & Xu, Q. (2018). Direct tensile properties of engineered cementitious composites: A review. Construction and Building Materials, 165, 346-362.

[32] Curosu, I., Liebscher, M., Mechtcherine, V., Bellmann, C., & Michel, S. (2017). Tensile behavior of high-strength strain-hardening cement-based composites (HS-SHCC) made with high-performance polyethylene, aramid and PBO fibers. Cement and Concrete Research, 98, 71-81.

[33] He, S., Qiu, J., Li, J., & Yang, E. H. (2017). Strain hardening ultra-high performance concrete (SHUHPC) incorporating CNF-coated polyethylene fibers. Cement and Concrete Research, 98, 50-60.

487 [34] Lu, Z., Yao, J., & Leung, C. K. (2019). Using graphene oxide to strengthen the bond between PE fiber and
488 matrix to improve the strain hardening behavior of SHCC. Cement and Concrete Research, 126, 105899.

489 [35] Li, V. C., Bos, F. P., Yu, K., McGee, W., Ng, T. Y., Figueiredo, S. C., ... & Kruger, P. J. (2020). On the emergence
490 of 3D printable engineered, strain hardening cementitious composites (ECC/SHCC). Cement and Concrete
491 Research, 132, 106038.

492 [36] Qian, S., & Li, V. C. (2008). Simplified inverse method for determining the tensile properties of strain
493 hardening cementitious composites (SHCC). Journal of Advanced Concrete Technology, 6(2), 353-363.

494 [37] Huang, B. T., Li, Q. H., Xu, S. L., Liu, W., & Wang, H. T. (2018). Fatigue deformation behavior and fiber
495 failure mechanism of ultra-high toughness cementitious composites in compression. Materials & Design, 157,
496 457-468.

497 [38] Huang, B. T., Li, Q. H., Xu, S. L., & Li, C. F. (2017). Development of reinforced ultra-high toughness
498 cementitious composite permanent formwork: experimental study and digital image correlation analysis.
499 Composite Structures, 180, 892-903.

500 [39] Fischer, G., & Li, V. C. (2003). Deformation behavior of fiber-reinforced polymer reinforced engineered
501 cementitious composite (ECC) flexural members under reversed cyclic loading conditions. ACI Structural
502 Journal, 100(1), 25-35.

503 [40] Yuan, F., Pan, J., & Leung, C. K. Y. (2013). Flexural behaviors of ECC and concrete/ECC composite beams
504 reinforced with basalt fiber-reinforced polymer. Journal of Composites for Construction, 17(5), 591-602.

505 [41] Cai, J., Pan, J., & Zhou, X. (2017). Flexural behavior of basalt FRP reinforced ECC and concrete beams.
506 Construction and Building Materials, 142, 423-430.

507 [42] Li, V. C., & Leung, C. K. (1992). Steady-state and multiple cracking of short random fiber composites. Journal
508 of Engineering Mechanics, 118(11), 2246-2264.

509 [43] Yao, J., & Leung, C. K. (2019). A new physical model for empirical fiber snubbing effect in cementitious
510 composites based on large deflection beam theory. Cement and Concrete Composites, 96, 238-251.
511 [44] Xu, L. Y., Huang, B. T., Li, V. C., & Dai, J. G. (2022). High-strength high-ductility Engineered/Strain-
512 Hardening Cementitious Composites (ECC/SHCC) incorporating geopolymer fine aggregates. Cement and
513 Concrete Composites, 125, 104296.
514 [45] Xu, L. Y., Huang, B. T., Lao, J. C., Yao, J., Li, V. C., & Dai, J. G. (2023). Tensile over-saturated cracking of
515 Ultra-High-Strength Engineered Cementitious Composites (UHS-ECC) with artificial geopolymer aggregates.
516 Cement and Concrete Composites, 136, 104896.
517 [46] Xu, L. Y., Huang, B. T., & Dai, J. G. (2021). Development of engineered cementitious composites (ECC) using
518 artificial fine aggregates. Construction and Building Materials, 305, 124742.
519 [47] Yao, J., & Leung, C. K. (2020). Scaling up modeling of strain-hardening cementitious composites based on
520 beam theory: From single fiber to composite. Cement and Concrete Composites, 108, 103534.
521 [48] Wang, L., Yin, S., & Hua, Y. (2021). Flexural behavior of BFRP reinforced seawater sea-sand concrete beams
522 with textile reinforced ECC tension zone cover. Construction and Building Materials, 278, 122372.
523 [49] Xu, L. Y., Huang, B. T., Lan-Ping, Q., & Dai, J. G. (2022). Enhancing long-term tensile performance of
524 Engineered Cementitious Composites (ECC) using sustainable artificial geopolymer aggregates. Cement and
525 Concrete Composites, 133, 104676.
526 [50] Xu, L. Y., Huang, B. T., Lao, J. C., & Dai, J. G. (2022). Tailoring strain-hardening behavior of high-strength
527 Engineered Cementitious Composites (ECC) using hybrid silica sand and artificial geopolymer aggregates.
528 Materials & Design, 220, 110876.
529 [51] Zhu, J. X., Xu, L. Y., Huang, B. T., Weng, K. F., & Dai, J. G. (2022). Recent developments in Engineered/Strain-
530 Hardening Cementitious Composites (ECC/SHCC) with high and ultra-high-strength. Construction and

Building Materials, 342, 127956.

[52] Huang, B. T., Zhu, J. X., Weng, K. F., Li, V. C., & Dai, J. G. (2022). Ultra-high-strength engineered/strain-hardening cementitious composites (ECC/SHCC): Material design and effect of fiber hybridization. Cement and Concrete Composites, 129, 104464.

[53] Xu, L. Y., Huang, B. T., & Dai, J. G. (2022). Utilization of Artificial Geopolymer Aggregates in High-Strength Engineered Cementitious Composites (HS-ECC). In International Conference on Strain-Hardening Cement-Based Composites (pp. 23-33). Cham: Springer International Publishing

[54] Li, Y., Guan, X., Zhang, C., & Liu, T. (2020). Development of high-strength and high-ductility ECC with saturated multiple cracking based on the flaw effect of coarse river sand. Journal of Materials in Civil Engineering, 32(11), 04020317.

[55] Yoo, D. Y., Oh, T., Kang, M. C., Kim, M. J., & Choi, H. J. (2021). Enhanced tensile ductility and sustainability of high-strength strain-hardening cementitious composites using waste cement kiln dust and oxidized polyethylene fibers. Cement and Concrete Composites, 120, 104030.

[56] Yoo, D. Y., & Banthia, N. (2022). High-performance strain-hardening cementitious composites with tensile strain capacity exceeding 4%: A review. Cement and Concrete Composites, 125, 104325.

[57] Kim, M. J., Choi, H. J., Shin, W., Oh, T., & Yoo, D. Y. (2021). Development of impact resistant high-strength strain-hardening cementitious composites (HS-SHCC) superior to reactive powder concrete (RPC) under flexure. Journal of Building Engineering, 44, 102652.

[58] Li, P., Chen, Y., & Yuan, F. (2023). Stress-strain behavior of ECC-GFRP spiral confined concrete cylinders. Journal of Building Engineering, 63, 105473.

[59] Huang, B. T., Wang, Y. T., Wu, J. Q., Yu, J., Dai, J. G., & Leung, C. K. (2021). Effect of fiber content on mechanical performance and cracking characteristics of ultra-high-performance seawater sea-sand concrete

(UHP-SSC). Advances in Structural Engineering, 24(6), 1182-1195.

[60] Bi, Y., Yang, C., Zhu, F., Chen, J., & Pan, Y. (2023). Study on the freeze–thaw cycles and carbonization of ultra-high molecular weight polyethylene fiber reinforced engineered cementitious composite for link slab. Construction and Building Materials, 400, 132371.

[61] Ding, Y., Liu, J. P., & Bai, Y. L. (2020). Linkage of multi-scale performances of nano-CaCO3 modified ultra-high performance engineered cementitious composites (UHP-ECC). Construction and Building Materials, 234, 117418.

[62] Gong, T., Curosu, I., Liebold, F., Vo, D. M., Zierold, K., Maas, H. G., ... & Mechtcherine, V. (2020). Tensile behavior of high-strength, strain-hardening cement-based composites (HS-SHCC) reinforced with continuous textile made of ultra-high-molecular-weight polyethylene. Materials, 13(24), 5628.

[63] Huang, B. T., Wu, J. Q., Yu, J., Dai, J. G., & Leung, C. K. (2020). High-strength seawater sea-sand Engineered Cementitious Composites (SS-ECC): Mechanical performance and probabilistic modeling. Cement and Concrete Composites, 114, 103740.

[64] ASTM C469 / C469M-14. (2014). Standard Test Method for Static Modulus of Elasticity and Poisson's Ratio of Concrete in Compression, ASTM International, West Conshohocken, PA.

[65] Japan Society of Civil Engineers. (2008). Recommendations for design and construction of high performance fiber reinforced cement composites with multiple fine cracks (HPFRCC). Concrete Engineering Series No. 82.

[66] Wu, H., Yu, J., Du, Y., & Li, V. C. (2021). Mechanical performance of MgO-doped engineered cementitious composites (ECC). Cement and Concrete Composites, 115, 103857.

[67] Yu, J., Wu, H. L., & Leung, C. K. (2020). Feasibility of using ultrahigh-volume limestone-calcined clay blend to develop sustainable medium-strength Engineered Cementitious Composites (ECC). Journal of Cleaner Production, 262, 121343.

575 [68] Wu, H. L., Zhang, D., Ellis, B. R., & Li, V. C. (2018). Development of reactive MgO-based Engineered
576 Cementitious Composite (ECC) through accelerated carbonation curing. Construction and Building Materials,
577 191, 23-31.

578 [69] Wu, H. L., Yu, J., Zhang, D., Zheng, J. X., & Li, V. C. (2019). Effect of morphological parameters of natural
579 sand on mechanical properties of engineered cementitious composites. Cement and Concrete Composites, 100,
580 108-119.

581 [70] Yu, J., Li, H., Leung, C. K., Lin, X., Lam, J. Y., Sham, I. M., & Shih, K. (2017). Matrix design for waterproof
582 engineered cementitious composites (ECCs). Construction and Building Materials, 139, 438-446.

583 [71] Lao, J. C., Huang, B. T., Fang, Y., Xu, L. Y., Dai, J. G., & Shah, S. P. (2023). Strain-hardening alkali-activated
584 fly ash/slag composites with ultra-high compressive strength and ultra-high tensile ductility. Cement and
585 Concrete Research, 165, 107075.

586 [72] Peng, K. D., Huang, J. Q., Huang, B. T., Xu, L. Y., & Dai, J. G. (2023). Shear strengthening of reinforced
587 concrete beams using geopolymer-bonded small-diameter FRP bars. Composite Structures, 305, 116513.

588 [73] Yang, X., Gao, W. Y., Dai, J. G., & Lu, Z. D. (2020). Shear strengthening of RC beams with FRP grid-reinforced
589 ECC matrix. Composite Structures, 241, 112120.

590 [74] GB 50666-2011. (2011). Code for construction of concrete structures. Ministry of Housing and Urban-Rural
591 Development of the People's Republic of China, Beijing, China. (in Chinese)

592 [75] Huang, B. T., Wu, J. Q., Yu, J., Dai, J. G., Leung, C. K., & Li, V. C. (2021). Seawater sea-sand
593 engineered/strain-hardening cementitious composites (ECC/SHCC): Assessment and modeling of crack
594 characteristics. Cement and Concrete Research, 140, 106292.

595 [76] Huang, B. T., Dai, J. G., Weng, K. F., Zhu, J. X., & Shah, S. P. (2021). Flexural Performance of UHPC–
596 Concrete–ECC Composite Member Reinforced with Perforated Steel Plates. Journal of Structural Engineering,

147(6), 04021065.

[77] Japan Society of Civil Engineers. (2008). Recommendations for design and construction of ultra-high-strength fiber reinforced concrete structures -Draft. (in Japanese)

[78] American Concrete Institute. (2014). ACI318, Building Code Requirements for Structural Concrete (ACI 318M-14) and Commentary (ACI 318RM-14).